Investigations into modifications of neuromuscular physiology by axonal transport disruptions in *Drosophila* SOD1 mutants

Tristan C. D. G. O'Harrow[1*†], Atsushi Ueda[1*], Xiaomin Xing[1*‡], Chun-Fang Wu[1]

[1] Department of Biology, University of Iowa, Iowa City, IA 52242, USA

* Equal contribution

[†] Current address: Raymond G. Perelman Center for Cellular and Molecular Therapeutics, The Children's Hospital of Philadelphia, Philadelphia, PA 19104, USA

[‡] Current address: Department of Pharmacology, School of Medicine, University of California, Davis, CA, 95616

ABSTRACT

The reactive oxygen species (ROS)-scavenging enzyme Cu/Zn superoxide dismutase (SOD1) is an evolutionarily conserved mechanism for the maintenance of oxidative homeostasis, and missense mutations in the human SOD1 gene are associated with the motor neuron degenerative disease amyotrophic lateral sclerosis (ALS). Mutations in the *Drosophila melanogaster* SOD1 gene (*Sod*) shorten fly lifespan, attenuate motor function, and induce developmental mortality. We have previously found morphological and physiological defects at the neuromuscular junctions (NMJs) of hypomorphic Sod^{n108} and ALS model Sod^{G85R} mutant larvae. Here, we report genetic interactions causing striking modifications of *Sod* mutant phenotypes by mutations in the gene *Prickle* (*Pk*), which are linked to planar cell polarity, epilepsy, and axonal transport disruptions. *Pk* is expressed as two isoforms *prickle-spiny-legs* (*sple*) and *prickle-prickle* (*pk*), which are each suppressed by specific hypomorphic mutations (*sple1* and *pk1*). Interestingly, *Sod* phenotypes are distinctly modified depending on both the *Pk* isoform suppressed, and whether said suppression is heterozygous or homozygous. Heterozygous *sple1* and *pk1* improved the developmental survival of *Sod* mutants, whereas homozygous *sple1* and *pk1* drastically increased mortality. Further, only heterozygous *sple1* and *pk1* clearly ameliorated morphological defects at the neuromuscular junctions of *Sod* mutant larvae. Pharmacological treatment of *Sod* mutants reveals allele-specific motor neuron terminal hyperexcitability, characterized by synaptic transmissions of

32 extended duration and abnormal presynaptic Ca^{2+} transients. Heterozygous *sple1* mutation
33 suppresses this *Sod* mutant terminal hyperexcitability, but *pk1* does not. We reversed this
34 suppressive effect of *sple1* by pharmacological blockade of Ca^{2+}-activated K^+ channel
35 *slowpoke*. Altogether, this study builds on our prior knowledge of *Sod* mutant development
36 and physiology to show that axonal transport-linked gene mutations strikingly modify *Sod*
37 mutant phenotypes, providing strong evidence for a role of intracellular transport in
38 alterations of neuromuscular morphology and physiology by SOD1 mutations.
39
40 **INTRODUCTION**
41 The ROS-scavenging enzyme Cu/Zn superoxide dismutase (SOD1) is highly
42 conserved across phyla, and is expressed in a wide variety of tissues (Uhlén et al., 2015).
43 Consequently, mutations in the gene encoding SOD1 have pervasive consequences for
44 physiology, developmental viability, and organismal longevity (Phillips et al., 1989).
45 Research continues to reveal defects in motor neuron development and physiology associated
46 with mutations in the SOD1 gene, including hypomorphic mutations and mutations linked to
47 familial amyotrophic lateral sclerosis (FALS) (Rosen et al., 1993).
48 Reactive oxygen species (ROS) are known to behave as signaling molecules to play a
49 wide variety of roles in healthy neuronal development and physiology (Thannickal &
50 Fanburg, 2000; Milton & Sweeney, 2011). During neurodevelopment, ROS modify the
51 biochemistry of cytoskeletal components to influence their dynamics and structure (Wilson &
52 González-Billaut, 2015; Munnamalai & Suter, 2009). The reactive superoxide anion (O_2^-) has
53 also been shown to regulate synaptic plasticity (Klann et al., 1998; Massaad & Klann, 2011).
54 In *Drosophila* larval motor neurons, oxidative stress influences synaptic structure and
55 transmission (Sanya et al., 2002), and regulates activity-dependent neuronal plasticity
56 (Oswald et al., 2018).
57 Loss of SOD1 function due to genetic mutation allows for oxidative stress in excess of
58 physiological levels. Resulting physiological disruptions include the misfolding of proteins
59 (Berlett & Stadtman, 1997), peroxidation of lipids (Altan et al. 2003), and alteration of
60 nucleic acids (Ali et al., 1996; Aitken & Krausz, 2001). High oxidative stress affects
61 neurodevelopment by disrupting cytoskeletal structures (Landino et al., 2002; Munnamalai &
62 Suter, 2009). SOD1 has been shown to support axon outgrowth and survival, and oxidative

63 stress induced by loss of SOD1 or treatment with a redox toxin triggers neurodegeneration.
64 (Fischer & Glass, 2010). Further, SOD1 knockout mice display NMJ neurotransmission
65 impairments and neuromuscular degeneration (Shi et al., 2014). The *n108* allele (Campbell et
66 al., 1985) of the *Drosophila* gene for SOD1 (*Sod*) is functionally null, and *n108* mutant larvae
67 and flies display hypersensitivity to oxidative stress (Phillips et al., 1989). The adults also
68 exhibit severely reduced lifespans (Phillips et al., 1989) and motor defects (Ruan & Wu,
69 2008). We have also previously shown that *n108* mutant larvae display altered synaptic
70 transmission at the neuromuscular junction, and supernumerary axon discharges (Ueda et al.,
71 *manuscript in preparation*), and defective neurotransmission in the adult giant fiber escape
72 circuit (Ueda et al., 2021).
73 Through mechanisms that remain to be clarified, SOD1 is linked to FALS when
74 specific amino acid substitutions are present. Mouse, *C. elegans*, and *Drosophila* models
75 expressing ALS-linked mutant SOD1 exhibit motor dysfunction or lethal paralysis (Wang et
76 al., 2008; Wang et al., 2009; Watson et al., 2008; Sahin et al., 2017; Agudelo et al., 2020).
77 Prior to detectable neurodegeneration, ALS mutant SOD1 impacts neurodevelopment and cell
78 metabolism. ALS mutant SOD1 localizes to actin structures, altering growth cone dynamics
79 and eventual neuronal morphology (Osking et al., 2019). Misfolded mutant SOD1 protein also
80 co-localizes with mitochondria in the axons of murine motor neuron, where mitochondrial
81 morphology is altered (Vande Velde et al., 2011) and mitochondrial Ca^{2+} buffering capacity is
82 defective (Damiano et al., 2006). The *Drosophila* ALS-linked *Sod* mutant *G85R* displays
83 defective larval locomotion, and consistently fails to eclose from the pupal stage (Held et al.,
84 2019; Sahin et al., 2017). *G85R* larvae also display proprioceptor neuron defects and
85 associated motor circuit dysfunction (Held et al., 2019).
86 In a separate report, we have characterized *Sod* mutant allele-dependent defects in
87 NMJ physiology and synaptic morphology (Ueda et al., Manuscript in preparation). In
88 screening for modifiers of synaptic transmission in *Drosophila Sod* mutants, we fortuitously
89 found genetic interactions between *Sod* and the planar cell polarity (PCP) and axonal
90 transport-linked gene *prickle* (*pk*) (Gubb & García-Bellido, 1982; Gray et al., 2011; Lin &
91 Gubb, 2009; Tree et al., 2002). *pk* is expressed in *Drosophila* in the form of the Pk^{Pk} (Prickle
92 Prickle) and Pk^{Sple} (Prickle Spiny-legs) isoforms. Isoform-specific loss-of-function mutants
93 (*pk1* and *sple1*, Gubb et al., 1999) display distinctly altered microtubule-mediated transport

94 and microtubule dynamics in larval motor axons, with related changes in neuronal excitability
95 (Ehaideb et al., 2014; Ehaideb et al., 2016). We have previously found that *pk1* and *sple1*
96 mutant larvae exhibit alterations in motor neuron development and synaptic transmission that
97 may be downstream of axon transport modifications (Ueda et al., 2022).
98 Here, we report the findings that *pk* isoform loss-of-function (LOF) mutations either
99 improve or reduce the developmental viability of *Sod* mutant *Drosophila* pupae in a genetic
100 dosage-dependent manner. Similarly, only heterozygous *pk* LOF suppresses NMJ morphology
101 defects in *Sod* mutants. We also demonstrate that *pk* LOF induces allele-specific alterations
102 *Sod* mutant NMJ transmission. Additionally, we show that selective pharmacological
103 blockade of ion channels reveals NMJ terminal hyperexcitability in Sod^{G85R}, and that this
104 phenotype is suppressed by partial LOF of the Pk^{Sple} isoform of *pk*. This work therefore
105 demonstrates that dysregulations of development and neuromuscular physiology induced by
106 *Sod* mutation can be altered by *pk* isoform dose manipulation, indicating potential roles of
107 modified intracellular transport in the generation of *Sod* mutant phenotypes.
108

109 **MATERIALS & METHODS**

110 Fly stocks

111 Flies and larvae were housed in bottles containing a cornmeal-agar medium (Frankel
112 & Brousseau, 1968), supplemented with 3g of yeast paste prepared as a 1:1 mixture of ddH_2O
113 and active dry yeast (Red Star Yeast Co., LLC). Flies were reared at a room temperature of 22
114 ± 1ºC. The *Sod* mutants examined were those of alleles *n108* (Phillips et al., 1989) (gift from
115 John Phillips, University of Guelph, Ontario, Canada) and *G85R* (Şahin et al. 2017) (gift from
116 Barry Ganetzky, University of Wisconsin-Madison, USA). The wild-type control strain used
117 for Figures 1, 2, 3, and 4 was Canton-S (CS). For experiments in which a motor neuron
118 membrane tag was needed, the stock used carried a chr. II *UAS-CD8-GFP* recombined with a
119 chr. II motor neuron GAL4 driver (Brand & Perrimon, 1993), either *C164-Gal4* (Torroja et
120 al., 1999) or *OK371-Gal4* (Mahr and Aberle, 2006). The original recombined *OK371-Gal4*
121 *UAS-CD8-GFP* (*OK371::CD8-GFP*) was obtained from the National Centre for Biological
122 Sciences (Bangalore, Karnataka, India). *Sod* lines used to produce the data represented in
123 Figure 1 were balanced over a TM6 balancer with a dominant *Tubby* (*Tb*) marker (TM6, *Tb*).

124 The Pk^{Pk} and Pk^{Sple} lines used in this study have been documented previously (Ehaideb et al.,
125 2014). The wild-type control strain used for Figure 5 was the Oregon-R (OR) used in Ehaideb
126 et al. (2014). All *Pk;Sod* double-mutant lines were generated in the Wu lab by conventional
127 genetic crosses.

128 Developmental lethality studies

129 Housing and medium conditions for the developmental lethality study (Figure 1) were
130 identical to those described in the main "Fly stocks" section. Flies including 20-40 females
131 were used to seed each bottle. Counts of deaths and eclosions were performed 16-17 d. after
132 seeding. The TM6, *Tb* balancer carried by *Sod* heterozygous wandering 3rd instar larvae and
133 pupae was used to distinguish them from *Sod* mutant homozygotes. Dead larvae appear as
134 darkened corpses on the wall of the housing bottle. Dead pupae were entirely black, or
135 contained a mixture of dark and empty patches, as confirmed by transmitted light under a
136 dissection scope. Juvenile flies dead during eclosion were distinguished from flies in the
137 process of eclosing by a second observation 15-30 min after the first. Juvenile fly corpses
138 were also frequently darker than their live counterparts.

139 Larval preparations, vital staining, & immunohistochemistry

140 Wandering third instar larvae were dissected, as per the "fillet preparation method", in
141 HL 3.1 saline (Feng et al., 2004). HL3.1 used in immunohistochemistry or vital staining
142 experiments contained 0.1 mM Ca^{2+}. Tetramethylrhodamine (TMRM, $C_{25}H_{25}ClN_2O_7$) (Floryk
143 & Houštěk, 1999) vital staining of larval preps for mitochondria was done at 100 nM in HL
144 3.1 for 20 minutes (in a light-impermeable chamber to prevent TMRM photobleaching), after
145 which the bath was replaced with TMRM-free HL 3.1 before microscopy. Before antibody
146 staining, larval preps were fixed in 3.7% formaldehyde in HL 3.1 for 25-30 minutes. Fixed
147 preps were incubated with an FITC-conjugated goat antibody to HRP at 1:50 in phosphate
148 buffer saline, at 4ºC for 12-48 h. Anti-HRP (Jan & Jan, 1982) recognizes a neural
149 carbohydrate antigen in *Drosophila* (Kurosaka et al., 1991). For double-staining with anti-
150 HRP and anti-Dlg (monoclonal AB 4F3: Parnas et al., 2001) or anti-Futsch (monoclonal AB
151 22C10: Fujita et al., 1982; Zipursky et al., 1984) staining, fixed larval preps were incubated
152 with the primary monoclonal AB at 1:100 in phosphate buffer saline, at 4ºC for 12-48 h,
153 rinsed, and incubated in phosphate buffer saline containing anti-HRP(conj. FITC) and a
154 secondary TRITC-conjugated anti-mouse IgG antibody, both at 1:50. The 4F3 and 22C10

155 antibodies were obtained from the Developmental Studies Hybridoma Bank (DSHB)
156 (University of Iowa, Iowa City, IA, USA). The FITC-conjugated anti-HRP and TRITC-
157 conjugated anti-mouse IgG were obtained from Jackson ImmunoResearch Laboratories (West
158 Grove, PA, USA). Larval NMJ images, vital and fixed, were gathered on a Leica DM IL LED
159 inverted microscope (Leica Microsystems Inc., Buffalo Grove, IL, USA), using the Leica
160 Application Suite X software.

161 Larval NMJ morphology and mitochondrial distributions

162 Examination of *Sod* single-mutant NMJ morphology (Figure 2) was carried out in
163 muscles 4 (M4) and 13 (M13), in abdominal segments A3, A4, and A5, and quantifications
164 from the different segments were pooled. Examination of *Pk;Sod* double-mutant NMJ
165 morphology (Figure 4) was carried out in muscle 4 (M4) in abdominal segments A2, A4, and
166 A6, and quantifications from the different segments were pooled. Counts of boutons from M4
167 include only type Ib boutons. Ib and Is boutons and branches in M13 were quantified
168 separately. Counts of specific bouton morphologies ("unsegregated" boutons and large
169 terminal boutons) are from M4 (Ib). For branch counting, a branch was defined as a terminal
170 process carrying at least two boutons (Zhong et al., 1992). A bouton was described as
171 incompletely segregated ("unsegregated") if the width of the narrowest point on the neck
172 preceding it was greater than 80% of the width of the widest point on the bouton. If multiple
173 unsegregated boutons appeared in a row, it could be difficult count them. In these cases,
174 counts were conservative. A terminal bouton was determined to be the "largest" if it was
175 measurably larger than any other bouton on that branch, past the last branching point.

176 Electrophysiology

177 All electrophysiological recordings were based on published protocols, and performed
178 in HL3.1 saline (Feng et al., 2004) (Composition (mM): 70 NaCl, 5 KCl, 0.1 $CaCl_2$, 4 $MgCl_2$,
179 10 $NaHCO_3$, 5 trehalose, 115 sucrose, 5 HEPES) (pH adjusted to 7.1). Intracellular recording
180 of excitatory junction potentials (EJPs) was adapted from Ueda and Wu (2006). Recording of
181 extracellular focal EJPs (efEJPs) was shown in Ueda and Wu (2009) and Xing and Wu
182 (2018a,b). For nerve-evoked action potentials, 0.1 ms stimuli were applied to the cut end of
183 the segmental nerve through a suction pipette. To enable analysis of presynaptic terminal
184 excitability, we also performed electrotonic stimulation (Wu et al., 1978; Ganetzky & Wu,
185 1982; 1983). Briefly: Tetrodotoxin (TTX) was applied to block Na+ channels. To achieve

186 direct electrotonic stimulation of the terminal, a 1 ms stimulus was applied to the cut
187 segmental nerve, which was sucked into the stimulation electrode, nearly up to the entry point
188 into the muscle, so as to allow the stimulus to passively propagate to the terminal and
189 depolarize the endplate membrane (Lee et al., 2014). In this manner, CaV channels
190 were directly triggered by local depolarization, independent from invasion of axonal Na+
191 action potentials. Further, a significant portion of multiple K+ channel species, including
192 *Shaker* (Kv1), were blocked by co-application of 4-aminopyridine (4-AP) and
193 tetraethylammonium (TEA) (Jan & Jan, 1977; Singh & Wu, 1999). Electrotonic stimulation
194 of the larval NMJ with TTX, 4-AP, and TEA has been shown in Lee et al. (2014). Such
195 manipulations allow for the examination of terminal excitability driven by Ca2+ channels
196 with reduced repolarization regulation by a range of K+ channels, with the exclusion of
197 axonal potential interplay.

198 Statistics

199 Total mortalities per genotype (Figure 1) were compared using Fisher's exact test.
200 Counts of NMJ boutons and branches and of enlarged terminal and unsegregated boutons
201 (Figures 2 and 3) were examined with Kruskal-Wallis testing between all groups within
202 muscle # and parameter (eg. M4, boutons), followed by rank-sum (Mann-Whitney U) post
203 hoc between individual groups. EJP sizes were compared with one-way ANOVA (Figure 4B).
204 Plateau-like EJP durations were compared by F-test (Figure 4D). Counts of NMJ
205 mitochondrial macropunctae (Figure 6) were compared with Kruskal-Wallis testing followed
206 by rank-sum (Mann-Whitney U) post hoc.

207

208 **RESULTS**

209 Lethality of *Sod* mutants during different developmental stages

210 Lifespan defects in adult *Drosophila* homozygous for hypomorphic *Sod* allele *n108*
211 (Ruan & Wu 2008) and pupal lethality in homozygotes of *n108* and the ALS-linked point-
212 mutant allele *G85R* (Şahin et al., 2017) have been previously characterized. We further noted
213 that *n108* and *G85R* mutants exhibit lethality in different phases of the pupal stage (Figure
214 1B). While the majority of *n108* death occurred at eclosion from the pupal stage (Figure 1A,
215 lower-right image), over 90% of *G85R* individuals died during pupal development (Figure
216 1A, middle-right image), unable to develop to the eclosion stage. Both *Sod* mutants also

217 displayed mild levels larval lethality (Figure 1A, upper-right image), similar between the
218 alleles. By comparison, *Drosophila* of control strains CS and *w1118* exhibited only very small
219 levels of developmental lethality that were greatly exceeded by the significant lethality in the
220 *Sod* mutants ($p < 0.001$). Heterozygous *Sod* mutants (*n108*/+ and *G85R*/+) did not differ in
221 lethality from the control strains (Supplemental Table 1), indicating a lack of phenotypic
222 dominance of *Sod* mutant lethality.
223 We found that the developmental lethality of *n108* and *G85R* mutants was modified by
224 mutations in *prickle*. Two copies of either the *pk1* or the *sple1* allele conferred full
225 developmental lethality to *n108* mutants, but unlike the lethality profile of the *n108* single-
226 mutant that generally died at eclosion, the *pk1*;*n108* and *sple1*;*n108* double-mutants died
227 during pupal development. *pk1*;*G85R* and *sple1*;*G85R* double-mutants remained as fully
228 lethal as the *G85R* single mutant, although rate of progression to eclosion was marginally
229 increased. Crucially, one copy of either *pk* mutant allele had the opposite effect: *Sod* mutant
230 lethality was suppressed. One copy of *pk1* (*pk1*/+;*n108*) lowered the overall rate of *n108*
231 lethality below 50%. A copy of *sple1* (*sple1*/+;*n108*) was even more effective, with lethality
232 reduced below 30%. Single copies of *pk1* and *sple1* (*pk1*/+;*G85R* and *sple1*/+;*G85R*)
233 conferred to *G85R* mutants rates of survival to adulthood of approx. 10% and 14%
234 respectively. These small proportions are notable when compared to the complete pre-
235 eclosion lethality of the *G85R* single mutant.
236
237 <u>Altered larval neuromuscular junction morphology</u>
238 The *Sod* mutants displayed mild alterations in NMJ outgrowth, that were readily visible in
239 counts of boutons per NMJ (Figure 2B). Counts of Ib branches and boutons in M4 and M13 in
240 *G85R* yielded distributions that were not significantly different from WT. While the increase
241 in *G85R* M13 Is branches was nonsignificant, the numbers of Is boutons were significantly
242 increased compared to WT ($p < 0.05$). NMJ outgrowth was increased in *n108* compared to
243 WT, with more more Ib boutons in M4 ($p < 0.05$) and M13 ($p < 0.001$), more Ib branches on
244 M13 ($p < 0.01$), and a visible but nonsignificant increase in numbers of M4 Ib branches
245 (Figure 2B). Where *n108* NMJ complexity was significantly greater than WT, it was also
246 significantly increased compared to *G85R*, indicating physiological differences between
247 mutants with the loss-of-function allele and those with the ALS-linked allele.

248 Both *Sod* mutants displayed increases in numbers of unsegregated boutons per M4 Ib branch
249 compared to WT (*G85R*: $p < 0.001$, *n108*: $p < 0.05$) (Figure 2C). Similarly, terminal boutons
250 that were enlarged compared to other boutons on the same M4 Ib branch appeared more
251 frequently in both *Sod* mutants than in WT (*G85R*: $p < 0.001$, *n108*: $p < 0.01$) (Figure 2C).
252
253 Unlike the *Sod* single-mutants, phenotypes of NMJ complexity (M4, Ib) in Pk^{Pk}, Pk^{Sple}, and
254 their double mutants with *G85R* were most visible in changes to the numbers of branches per
255 NMJ. Compared to WT, Pk^{Pk};*G85R* displayed significantly more boutons ($p < 0.01$), and
256 Pk^{Sple};*G85R* displayed significantly fewer ($p < 0.01$). Both double-mutants displayed fewer
257 branches than either corresponding *Pk* single-mutant (both $p < 0.001$), and Pk^{Sple};*G85R*
258 displayed a number of boutons similar to the *G85R* single-mutant, strikingly fewer than the
259 Pk^{Sple} single-mutant. ($p < 0.001$). Both *Pk* single-mutants displayed slightly more boutons
260 than WT (both $p < 0.05$). None of the *Pk* single-mutants or *Pk*;*G85R* double-mutants
261 displayed a number of unsegregated boutons that was significantly different from WT, nor
262 was there a clear difference between WT and the *Pk* single-mutants in the rate at which
263 terminal boutons were enlarged. However, both *Pk*;*G85R* double-mutants displayed enlarged
264 terminal boutons at rates lower than *G85R*, but still greater than WT (both $p < 0.01$).
265
266 <u>Genetic interaction between *Sod* and *Pk* in motor neuron excitability and synaptic</u>
267 <u>transmission</u>
268 In light of the NMJ morphological defects manifested in *Sod* through its interaction with *Pk*
269 mutations, we examined neuromuscular transmission for related defects. When the motor
270 axon bundle was stimulated with 0.1 ms pulses in HL3.1 saline containing 0.2 mM Ca2+, we
271 detected reliable EJP responses in *Sod* and *Pk* mutant larvae. In *Sod* mutants (hypomorphic
272 alleles *n108* and *x39*/*n108*, as well as the ALS-related *G85R* allele), EJP response upon nerve
273 stimulation was similar to that in WT ($p > 0.05$, Figure 4B). EJP size in the *Pk* alleles of *Pk*
274 (*Pk1* and *Pk30*, data combined in Figure 4) was comparable to WT, while EJP size was
275 significantly decreased in the mutants of the *Sple* allele ($p<0.05$, One-Way ANOVA).
276 However, the double-mutant Pk^{Pk1};Sod^{G85R} showed unusually large EJPs (Figure 4B, $p < 0.05$,
277 One-Way ANOVA). Abnormal synaptic transmission can be attributed to alterations in ion

278 channels participating in regulation of presynaptic terminal membrane depolarization to
279 control Ca^{2+} influx that triggers release of synaptic vesicles from presynaptic terminals.
280
281 Sod^{G85R} allele-specific motor terminal hyperexcitability
282 *Sod* mutant axonal excitability having been studied (Figure 3) (Ueda et al., In
283 preparation), we examined the isolated electrophysiological properties of the *Sod* mutant
284 larval NMJ using a previously established protocol of direct electrotonic stimulation of the
285 axon terminal, after silencing the axon Na+ spikes via TTX (Ganetzky & Wu, 1982, 1983;
286 Ueda & Wu 2009; Lee et al., 2013). Varying intensities of direct electrotonic stimulation of
287 the presynaptic terminal revealed no clear qualitative differences between *G85R*, *n108*, and
288 WT in loose-patch focal recording (see methods) of efEJP (extracellular focal excitatory
289 junction potentials) from single synaptic boutons (Figure 4A). Exposure of the larval
290 preparation to the *Shaker* K_V channel blocker 4-aminopyridine (4-AP, 200 nM) induced NMJ
291 hyperexcitability in *G85R* larvae that was typically absent under the same condition in *n108*
292 and WT. The *Shaker* blockade-induced hyperexcitability of *G85R* manifested in the form of a
293 shoulder-like extension of the efEJP (Figure 4B). We quantified this characteristic with a
294 measurement of the duration at 20% amplitude beyond the baseline (Figure 6). A
295 presynaptically expressed Ca^{2+} indicator (GCaMP6f) also communicated the state of Ca^{2+}
296 currents in the recorded synaptic boutons during evoked neurotransmission, which revealed
297 that *G85R* also exhibited brief presynaptic Ca^{2+} currents in response to electrotonic stimuli in
298 the presence of 4-AP. In fact, we found that every extended efEJP was accompanied by a
299 spike in presynaptic GCaMP (Figure 4B, Figure 6). Given this consistent association between
300 augmented presynaptic Ca^{2+} currents and modified postsynaptic response, we suspect that the
301 prolonged efEJP is elicited by prolonged neurotransmitter release from the presynaptic
302 terminal.
303 pk^{sple1} suppression of Sod^{G85R} hyperexcitability
304 The *sple1* null allele of *prickle* exerted a striking effect on the NMJ physiology of
305 *G85R*: One copy of *sple1* was sufficient to suppress both the efEJP extension and the
306 simultaneous presynaptic Ca^{2+} current amplification (Figure 5B, Figure 6). That the control
307 *sple1*/+ mutant larvae exhibit mild hyperexcitability in response to 4-AP reveals that the
308 genetic interaction between *G85R* and *sple1* is not simply the sum of opposing phenotypes.

309 Further, the suppressive interaction of *sple1/+* with *G85R* physiology is *pk* allele-dependent,
310 and does not arise from the combination of the *pk1* allele with *G85R* (Figure 5B, Figure 6).
311
312 **DISCUSSION**
313 Our study contrasts the loss-of-function *n108* allele of *Sod* with the ALS-linked *G85R*
314 allele, by demonstrating clear differences in the developmental stages at which the mutants of
315 each allele die. The contrast is further enhanced by differences between their neuromuscular
316 synapse morphologies. We found potential mechanistic links between abnormal distribution
317 of mitochondria in Sod^{G85R} and synaptic bouton enlargement (Ueda et al., Manuscript in
318 preparation), consistent with the striking interaction with *Pk*, known to affect axonal transport.
319 Further, following pharmacological blockade of Na+ and K+ currents in our
320 electrophysiological experiments, the remaining Ca2+ currents appeared to initiate more
321 physiological actions in Sod^{G85R}, in a manner suppressed by *sple1* mutation.
322 Developmental death in *Sod* mutants
323 This study of *Drosophila Sod* mutant lethality extends specificity and aspects of
324 mutational effects on the developmental stages in which deaths occur. Specifically, we
325 distinguish between death of the fully developed juvenile fly during eclosion from the pupal
326 casing, and death mid-pupal development, which is characterized by a pupal casing that
327 remains closed. As a result, we established allele-dependent developmental lethality
328 phenotypes. The *n108* lethality occurs largely during eclosion and may be due to physical
329 weakness of the juvenile. The vast majority of *G85R* death occurs during pupal development,
330 often prior to formation of adult morphology, as seen by a lack of red adult eyes visible
331 through the pupal casing of late-stage pupae (Bainbridge & Bownes, 1981).
332 Aberrant NMJ morphology and physiology
333 Overgrowth of the Sod^{n108} NMJ has been documented previously, and another
334 oxidative stress-sensitive mutant (*spinster*) was shown to have similar overgrowth. Further,
335 the two genes show synergistic interactions (Milton et al., 2011). The *G85R* larval NMJ has
336 also been characterized (Held et al., 2019) although the bouton number did not seem to differ
337 significantly from their control. In this study, we also found no clear difference in bouton
338 numbers, but striking bouton morphological alterations could be demonstrated in *G85R* larvae
339 (Figure 2A). Additional immunostaining of proteins constituting the presynaptic machinery,

340 such as synaptotagmin and dynamin (Estes et al., 1996), or postsynaptic elements such as
341 glutamate receptors (Harris & Littleton, 2015), could elucidate the functional relevance of the
342 unusual bouton morphologies in *Sod* mutants.

343 Mutant SOD1 is the most commonly identifiable risk factor in human patients with
344 familial ALS (Zarei et al., 2015). By exploiting the amenability of the *Drosophila* larval
345 neuromuscular preparation to the study of motor synapses at an early developmental stage, we
346 detect clear signs of synaptic physiology and morphology alterations in *Sod* mutants.
347 Additionally, abnormal distributions of synaptic mitochondria in *Sod,* and severe NMJ
348 phenotypes in *Sod* double-mutants with transport-affecting *Pk* mutations, suggest
349 dysfunctional transport may contribute to early SOD1-linked pathology. Our work therefore
350 adds to our understanding of phenotypes and mechanisms that will facilitate further studies to
351 uncover critical events leading to irreversible and terminal motor neuron degeneration in
352 ALS.

353

354 **References**

355 Aitken RJ, Krausz C. (2001) Oxidative stress, DNA damage, and the Y chromosome.
356 *Reproduction* 122: 497-506.
357 Akbergenova Y, Bykhovskaia M. (2007) Synapsin maintains the reserve vesicle pool and
358 spatial segregation of the recycling pool in *Drosophila* presynaptic boutons. *Brain*
359 *Research* 1178: 52-64.
360 Ali S, Jain SK, Abdulla M, Athar M. (1996) Paraquat induced DNA damage by reactive
361 oxygen species. *Biochemistry and Molecular Biology International* 39(1): 63-67.
362 Altan O, Pabuccuoglu A, Altan A, Konyalioglu S, Bayraktar H. (2003) Effect of heat stress
363 on oxidative stress, lipid peroxidation, and some stress parameters in broilers. *British*
364 *Poultry Science* 44(4): 545-550.
365 Bainbridge SP, Bownes M. (1981) Staging the metamorphosis of *Drosophila* melanogaster.
366 *J. Embryol. exp. Morph.* 66: 57-80.
367 Bassuk AG, Wallace RH, Buhr A, ..., Slusarski DC, Berkovic SF, El-Shanti HI. (2008) A
368 homozygous mutation in human PRICKLE1 causes an autosomal-recessive
369 progressive myoclonus epilepsy-ataxia syndrome. *The American Journal of Human*
370 *Genetics* 83: 572-581.
371 Berlett BS, Stadtman ER. (1997) Protein Oxidation in Aging, Disease, and Oxidative Stress.
372 *The Journal of Biological Chemistry* 272(33): 20313-20316.
373 Bilsland LG, Sahai E, Kelly G, Golding M, Greensmith L, Schiavo G. (2010) Deficits in
374 axonal transport precede ALS symptoms in vivo. *Proc Natl Acad Sci* 107(47):
375 20523-20528.
376 Brand AH, Perrimon N. (1993) Targeted gene expression as a means of altering cell fates
377 and generating dominant phenotypes. *Development* 118:401-415.

Campbell SH, Hilliker AJ, Phillips JP. (1985) Cytogenetic analysis of the *cSOD* microregion in *Drosophila melanogaster*. *Genetics* 112: 205-215.

Ehaideb SN, Iyengar A, Ueda A, Iacobucci GJ, Cranston C, Bassuk AG, Gubb D, Axelrod JD, Gunawardena S, Wu CF, Manak RJ. (2014) *prickle* modulates microtubule polarity and axonal transport to ameliorate seizures in flies. *Proc. Natl. Acad. Sci. USA* 111(30): 11187-11192.

Ehaideb SN, Wignall EA, Kasuya J, Evans WH, Iyengar A, Koerselman HL, Lilienthal AJ, Bassuk AG, Kitamoto T, Manak RJ. (2016) Mutation of orthologous prickle genes causes a similar epilepsy syndrome in flies and humans. *Annals of Clinical and Translational Neurology* 3 (9): 695-707.

Estes PS, Roos J, van der Bliek A, Kelly RB, Krishnan KS, Ramaswami M. (1996) Traffic of Dynamin within individual *Drosophila* synaptic boutons relative to compartment-specific markers *J. Neurosci.* 1996 16(17): 5443-5456.

Feng Y, Ueda A, Wu CF. (2004) A modified minimal hemolymph-like solution, HL3. 1, for physiological recordings at the neuromuscular junctions of normal and mutant Drosophila larvae. *Journal of Neurogenetics*, 18(2): 377-402.

Frankel, A., & Brousseau, G. (1968). Drosophila medium that does not require dried yeast. *Drosophila Information Service* 43, 184.

Ganetzky B, Wu CF. (1982) *Drosophila* mutants with opposing effects on nerve excitability: Genetic and spatial interactions in repetitive firing. *Journal of Neurophysiology* 47(3): 501-514.

Ganetzky B, Wu CF. (1983) Neurogenetic analysis of potassium currents in *Drosophila*: Synergistic effects on neuromuscular transmission in double mutants. *Journal of Neurogenetics* 1: 17-28.

Gubb D, García-Bellido A. (1982) A genetic analysis of the determination of cuticular polarity during development in *Drosophila melanogaster*. *J. Embryol. exp. Morph.* 68: 337-57.

Gubb D, Green C, Huen D, Coulson D, Johnson G, Tree D, Collier S, Roote J. (1999) The balance between isoforms of the Prickle LIM domain protein is critical for planar polarity in *Drosophila* imaginal discs. *Genes & Development* 13: 2315-2327.

Gray RS, Roszko I, Solnica-Krezel L. (2011) Planar cell polarity: coordinating morphogenetic cell behaviors with embryonic polarity. *Developmental Cell* 21: July 19, 2011.

Harris KP, Littleton T. (2015) Transmission, development, and plasticity of synapses. *Genetics* 201: 345-375.

Held A, Major P, Sahin A, Reenan RA, Lipscombe D, Wharton KA. (2019) Circuit dysfunction in SOD1-ALS model first detected in sensory feedback prior to motor neuron degeneration is alleviated by BMP signaling. *Neurobiology of Disease* 39(12): 2347-2364.

Jan LY, Jan YN. (1976a) Properties of the larval neuromuscular junction in *Drosophila melanogaster*. *J. Physiol.* 262: 189-214.

Jan LY, Jan YN. (1976b) L-glutamate as an excitatory transmitter at the *Drosophila* larval neuromuscular junction. *J. Physiol.* 262: 215-236.

Jan YN, Jan LY, Dennis MJ. (1977) Two mutations of synaptic transmission in *Drosophila. Proc. R. Soc. Lond. B.* 198: 87-108.

423 Jan LY, Jan YN. (1982) Antibodies to horseradish peroxidase as specific neuronal markers
424 in *Drosophila* and in grasshopper embryos. *Proc. Natl. Acad. Sci. USA* 79: 2700-
425 2704.
426 Katz B, Miledi R. (1967a) A study of synaptic transmission in the absence of nerve
427 impulses. *J. Physiol.* 192: 407-436.
428 Katz B, Miledi R. (1967b) Tetrodotoxin and neuromuscular transmission. *Proceedings of*
429 *the Royal Society B* 167 (1006): 8-22.
430 Klagges BRE, Heimbeck G, Godenschwege TA, Hofbauer A, Pflugfelder GO, Reifegerste
431 R, Reisch D, Schaupp M, Buchner S, Buchner E. (1996) Invertebrate synapsins: A
432 single gene codes for several isoforms in *Drosophila*. *J. Neurosci.* 16(10): 3154-
433 3165.
434 Kurdyak P, Atwood HL, Stewart BA, Wu CF. (1994) Differential physiology and
435 morphology of motor axons to ventral longitudinal muscles in larval *Drosophila. The*
436 *Journal of Comparative Neurology* 350: 463-472.
437 Kurosaka A, Yano A, Itoh N, Kuroda Y, Nakagawa T, Kawasaki T. (1991) The structure of
438 a neural specific carbohydrate epitope of horseradish peroxidase antiserum. *the*
439 *Journal of Biological Chemistry* 266(7): 4168-4172.
440 Lee J, Ueda A, Wu CF (2014) Distinct roles of *Drosophila cacophony* and *Dmca1D* Ca2+
441 channels in synaptic homeostasis: Genetic interactions with *slowpoke* Ca2+-activated
442 BK channels in presynaptic excitability and postsynaptic response. *Dev. Neurobiol.*
443 141: 4548-4557.
444 Lee J, Wu CF. (2010) Orchestration of Stepwise Synaptic Growth by K+ and Ca2+
445 Channels in *Drosophila*. *J. Neurosci.* 30(47): 15921-15833.
446 Lin YY, Gubb D. (2009) Molecular dissection of *Drosophila* Prickle isoforms distinguishes
447 their essential and overlapping roles in planar cell polarity. *Developmental Biology*
448 325: 386-399.
449 Mahr A, Aberle H. (2006) The expression pattern of the *Drosophila* vesicular glutamate
450 transporter: A marker protein for motoneurons and glutamatergic centers in the brain.
451 *Gene Expression Patterns* 6: 299-309.
452 Massaad CA, Klann E. (2011) Reactive Oxygen Species in the Regulation of Synaptic
453 Plasticity and Memory. *Antioxidants and Redox Signaling* 14(10): 2013-2054.
454 Mei X, Wu S, Bassuk AG, Slusarski DC. (2013) Mechanisms of *prickle1a* function in
455 zebrafish epilepsy and retinal neurogenesis. *Disease Models & Mechanisms* 6: 679-
456 688.
457 Milton VJ, Jarrett HE, Gowers K, Chalak S, Briggs L, Robinson IM, Sweeney ST. (2011)
458 Oxidative stress induces overgrowth of the *Drosophila* neuromuscular junction. *Proc*
459 *Natl Acad Sci* 108(42): 17521-17526.
460 Osking Z, Ayers JI, Hildebrandt R, Skruber K, Brown H, Ryu D, ... Vitriol EA. (2019) ALS-
461 linked SOD1 mutants enhance neurite outgrowth and branching in adult motor
462 neurons. *iScience* 11: 294-304.
463 Paemka L, Mahajan VB, Skeie JM, ..., Carvill GL, Manak RJ, Bassuk AG. (2013)
464 PRICKLE1 interaction with SYNAPSIN I reveals a role in autism spectrum
465 disorders. *PLOS ONE* 8 (12): e80737.
466 Parnas D, Haghighi P, Fetter RD, Kim SW, Goodman CS. (2001) Regulation of
467 postsynaptic structure and protein localization by the rho-type guanine nucleotide
468 exchange factor dPix. *Neuron* 32: 415-424.

469 Phillips JP, Campbell SD, Michaud D, Charbonneau M, Hilliker, AJ. (1989) Null mutation
470 of copper/zinc superoxide dismutase in Drosophila confers hypersensitivity to
471 paraquat and reduced longevity. *Proc Natl Acad Sci* 86(8): 2761-2765.
472 Rosen DR, Siddique T, Patterson D, Figlewicz DA, Sapp P, Hentati A, ... Brown RH Jr.
473 (1993) Mutations in Cu/Zn superoxide dismutase gene are associated with familial
474 amyotrophic lateral sclerosis. *Nature* 362: 59-62.
475 Ruan, H., & Wu, C. F. (2008). Social interaction-mediated lifespan extension of *Drosophila*
476 Cu/Zn superoxide dismutase mutants. *Proc Natl Acad Sci* 105(21): 7506-7510.
477 Şahin A, Held A, Bredvik K, Major P, Achilli TM, Kerson, AG, ... Reenan, R. (2017).
478 Human SOD1 ALS mutations in a *Drosophila* knock-in model cause severe
479 phenotypes and reveal dosage-sensitive gain- and loss-of-function components.
480 *Genetics* 205(2): 707-723.
481 Singh S, Wu CF. (1999) Ionic currents in larval muscles of *Drosophila. International*
482 *Review of Neurobiology* 43: 191-220.
483 Stewart BA, Atwood HL, Renger JJ, Wang J, Wu CF. (1994) Improved stability of
484 *Drosophila* larval neuromuscular preparations in haemolymph-like physiological
485 solutions. *J Comp Physiol A* 175: 179-191.
486 Thannickal VJ, Fanburg BL. (2000) Reactive oxygen species in cell signaling. *Am J Physiol*
487 *Lung Cell Mol Physiol* 279: L1005-L1028.
488 Torroja L, Packard M, Gorczyca M, White K, Budnik V. (1999) The *Drosophila* β-amyloid
489 precursor protein homolog promotes synapse differentiation at the neuromuscular
490 junction. *The Journal of Neuroscience* 19(18): 7793-7803.
491 Tree DRP, Shulman JM, Rousset R, Scott MP, Gubb D, Axelrod JD. (2002) Prickle
492 mediates feedback amplification to generate asymmetric planar cell polarity
493 signaling. *Cell* 109: 371-381.
494 Ueda A, Wu CF. (2006) Distinct frequency-dependent regulation of nerve terminal
495 excitability and synaptic transmission by I_A and I_K potassium channels revealed by
496 *Drosophila Shaker* and *Shab* mutations. *The Journal of Neuroscience* 26(23): 6238-
497 6248.
498 Ueda A, Wu CF. (2009) Role of *rut* adenylyl cyclase in the ensemble regulation of
499 presynaptic terminal excitability: Reduced synaptic strength and precision in a
500 *Drosophila* memory mutant. *J Neurogenet* 23: 185-199.
501 Vande Velde C, McDonald KK, Boukhedimi Y, ... Cleveland DW. (2011) Misfolded SOD1
502 Associated with Motor Neuron Mitochondria Alters Mitochondrial Shape and
503 Distribution Prior to Clinical Onset. *PLoS ONE* 6(7): e22031.
504 Vasin A, Zueva L, Torrez C, Volfson A, Littleton JT, Bykhovskaia M. (2014) Synapsin
505 regulates activity-dependent outgrowth of synaptic boutons at the *Drosophila*
506 neuromuscular junction. *J. Neurosci.* 34(32): 10554-10563.
507 Wang J, Farr GW, Zeiss CJ, Rodriguez-Gil DJ, Wilson JH, ... Horwich AL. (2008)
508 Progressive aggregation despite chaperone associations of a mutant SOD1-YFP in
509 transgenic mice that develop ALS. *Proc Natl Acad Sci* 106(5): 1392-1897.
510 Wang J, Farr GW, Hall DH, Li F, Furtak K, Dreier L, ... Horwich AL. (2009) An ALS-
511 Linked Mutant SOD1 Produces a Locomotor Defect Associated with Aggregation
512 and Synaptic Dysfunction When Expressed in Neurons of Caenorhabditis elegans.
513 *PLoS Genetics* 5(1): e1000350.

514 Xing X, Wu CF. (2018a) Unraveling synaptic GCaMP signals: Differential excitability and
515 clearance mechanisms underlying distinct Ca^{2+} dynamics in tonic and phasic
516 excitatory, and aminergic modulatory motor terminals in *Drosophila*. *eNeuro* 5(1):
517 e0362-17.2018 1-28
518 Xing X, Wu CF. (2018b) Inter-relationships among physical dimensions, distal–proximal
519 rank orders, and basal GCaMP fluorescence levels in Ca^{2+} imaging of functionally
520 distinct synaptic boutons at *Drosophila* neuromuscular junctions. *J Neurogenet*
521 32(3): 195-208.
522 Zarei S, Carr K, Reiley L, Diaz K, Guerra O, Fernandez Altamirano P, ... Chinea A. (2015)
523 A comprehensive review of amyotrophic lateral sclerosis. *Surgical Neurology*
524 *International* 6:171.
525 Zhong Y, Budnik V, Wu CF. (1992) Synaptic plasticity in *Drosophila* memory and
526 hyperexcitable mutants: role of cAMP cascade. *J Neurosci* 12(2): 644-651.
527 Zipursky SL, Venkatesh TR, Teplow DB, Benzer S. (1984) Neuronal development in the
528 *Drosophila* retina: Monoclonal antibodies as molecular probes. *Cell* 36: 15-26.

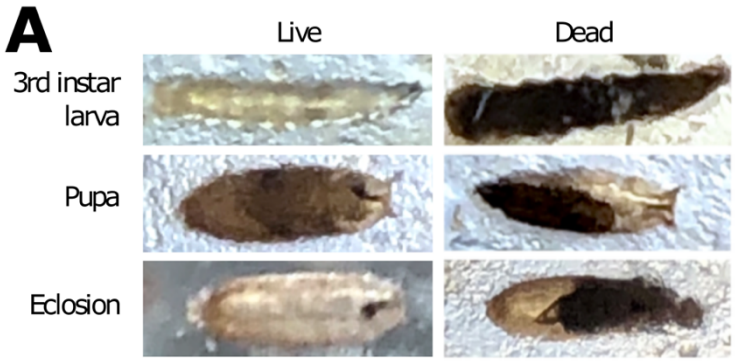
A
Live
Dead
3rd instar larva
Pupa
Eclosion

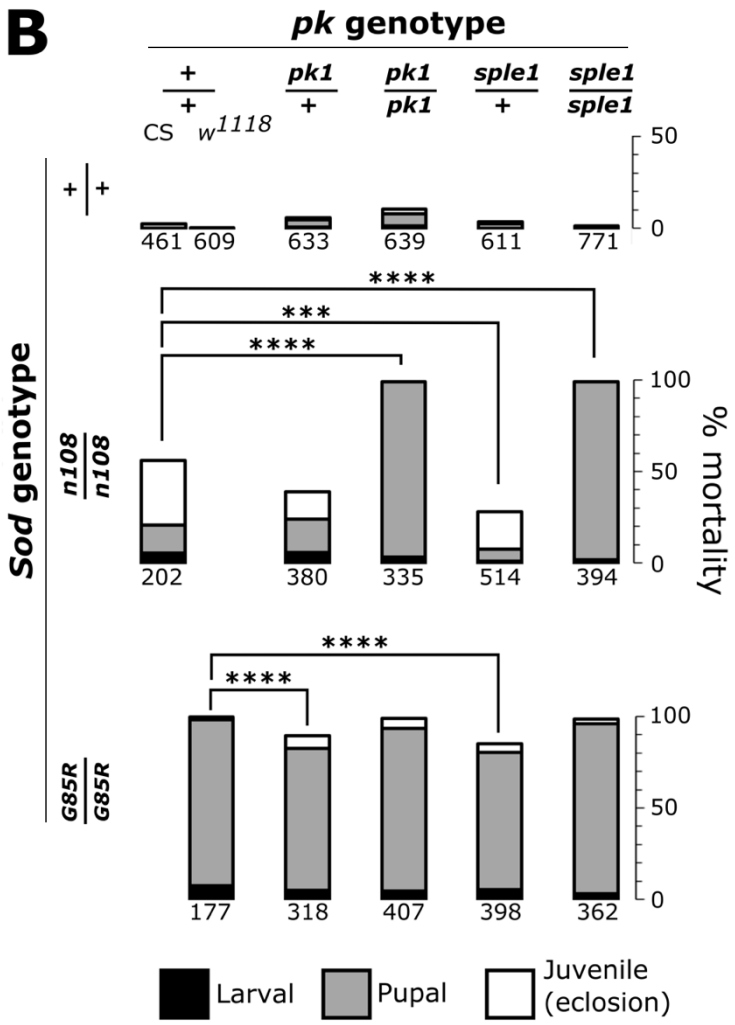
B
pk genotype
+ / +
CS
w1118
pk1 / +
pk1 / pk1
sple1 / +
sple1 / sple1
Sod genotype
+ | +
461 609 633 639 611 771
n108 / n108
202 380 335 514 394
G85R / G85R
177 318 407 398 362
****
***
****
****
****
50
0
100
50
0
100
50
0
% mortality
Larval
Pupal
Juvenile (eclosion)

Figure 1. Developmental lethality in *Sod* mutants is modified by *pk* mutations. (A) Representative images of live and dead larvae and pupae, an empty pupal casing left after successful eclosion of the juvenile fly, and the carcass of a juvenile dead during eclosion. (B) *Sod* mutant survival during development is improved by one copy of either *sple1* or *pk1*. Bars show percentages of individuals dead at the 3rd instar larval stage (black), during pupal development (gray), and at eclosion from the pupal casing (white). Genotypes shown are *Sod* mutants *G85R* and *n108*, *pk* mutants *pk1* and *sple1*, *pk1/+* and *sple1/+* heterozygotes, and double-mutants of those *Sod* and *pk* alleles. Both wild-type CS and *w1118* are included as controls due to differing genetic backgrounds of *G85R* and *n108*. *n* indicated below each bar. ***$P < 0.001$, ****$P < 0.0001$, Fisher's exact test. Statistics are for cumulative developmental mortality.

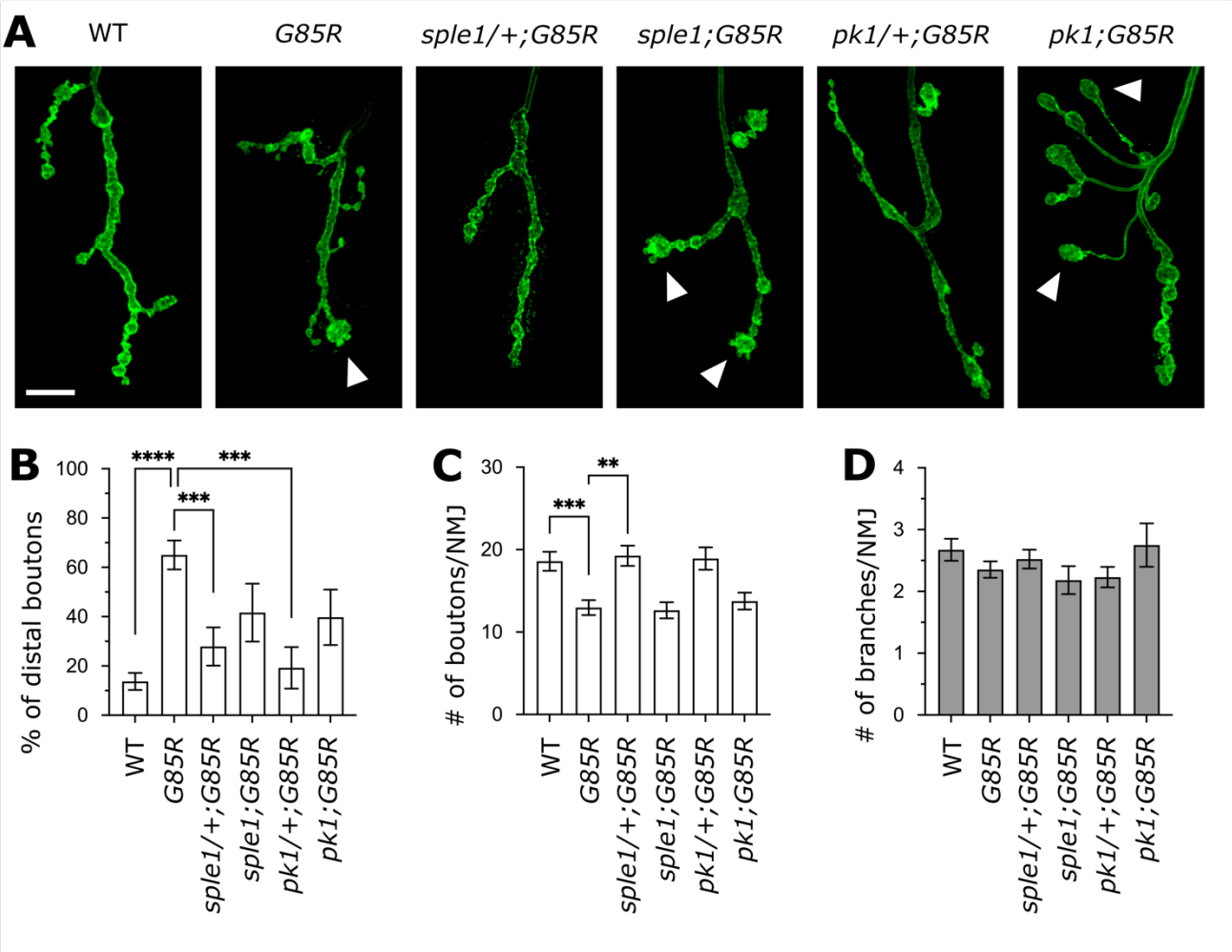

Figure 2. Heterozygous *prickle* loss-of-function suppresses Sod^{G85R} neuromuscular junction morphology defects. (A) Representative images of type Ib NMJs from muscle 4 in wild-type (WT), Sod^{G85R} (*G85R*), heterozygous and homozygous double-mutants of *sple1* with *G85R* (*sple1/+;G85R* and *sple1;G85R*), and heterozygous and homozygous double-mutants of *pk1* with *G85R* (*pk1/+;G85R* and *pk1;G85R*). Immunostaining shows presynaptic morphology (Anti-HRP). White arrows indicate *Sod* phenotypic enlarged distal boutons. Scale bar = 10 µm. (B) Percentage of distal synaptic boutons that are enlarged in each genotype (see methods). (C) Numbers of presynaptic boutons (see methods). (D) Numbers of presynaptic branches (see methods). Bars in B, C and D indicate mean, error bars indicates SEM. *N* of NMJ = WT: 46, *G85R*: 34, *sple1/+;G85R*: 23, *sple1;G85R*: 11, *pk1/+;G85R*: 13, *pk1;G85R*: 12. $^{**}P < 0.01$, $^{***}P < 0.001$, $^{****}P < 0.0001$, one-way ANOVA followed by Tukey's test.

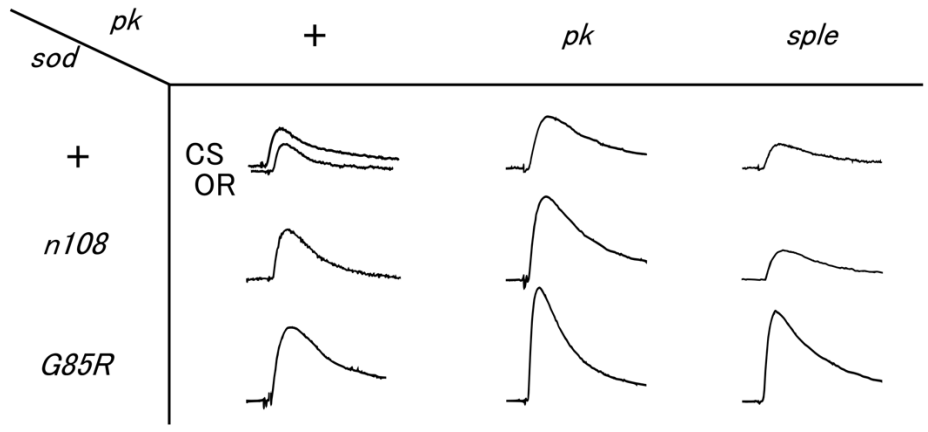

Figure 3. Homozygous *pk* mutations alter the size of excitatory junctional potentials (EJPs) from body wall muscles in *Sod* mutant larvae. Two different WT controls (CS and OR) are shown. EJPs were measured in HL3.1 saline containing 0.2 mM Ca^{2+}.

sod \ *pk*	+	*pk* / +	*pk*	*sple* / +	*sple*
+	OR 6.9 ± 1.2 (16) CS 11.9 ± 1.4 (22)	3.6 ± 0.7 (8)	14.8 ± 2.8 (12)	5.6 ± 0.9 (5)	6.4 ± 1.6 (16)
n108	15.3 ± 3.3 (7)	ND	22.0 ± 6.4 (5)	ND	8.0 ± 2.1 (6)
G85R	19.5 ± 3.4 (9)	ND	28.3 ± 4.3 (9)	24.6 ± 2.2 (6)	23.2 ± 2.5 (10)

Table 1. Muscle EJP size (mean ± SEM) in *Sod, pk,* and double mutant combinations. Wild-type CS is the control strain for *Sod* and wild-type OR is the control for *pk*. *N* of NMJs are indicated in parentheses. EJPs were measured in HL3.1 saline containing 0.2 mM Ca^{2+}.

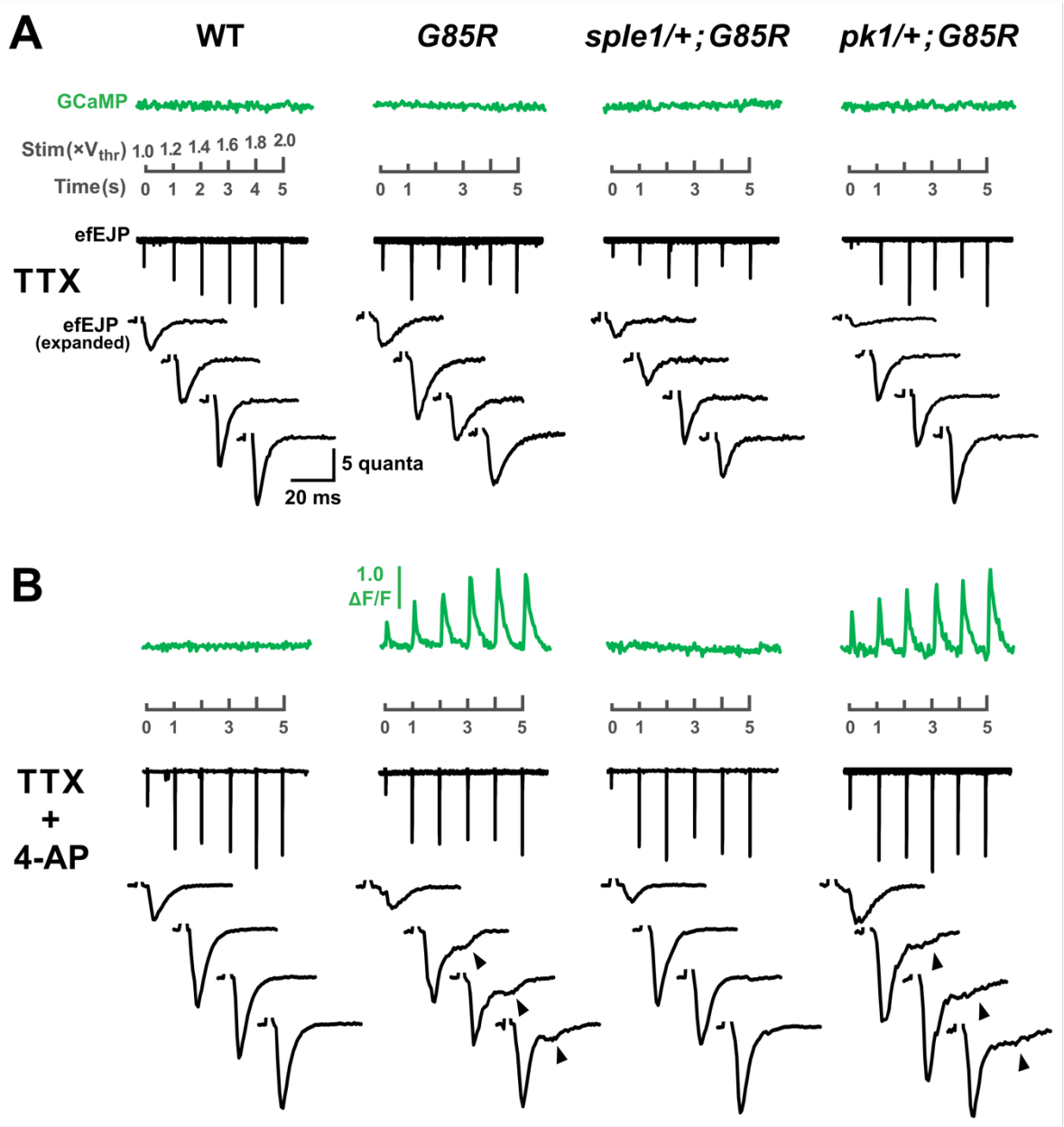
A
WT
G85R
sple1/+;G85R
pk1/+;G85R
GCaMP
Stim(×V$_{thr}$) 1.0 1.2 1.4 1.6 1.8 2.0
Time(s) 0 1 2 3 4 5
0 1 3 5
efEJP
TTX
efEJP
(expanded)
5 quanta
20 ms
B
1.0
ΔF/F
TTX
+
4-AP

Figure 4. Heterozygous *sple1* suppresses the NMJ terminal hyperexcitability of Sod^{G85R}. (A) efEJP of *sple1/+;G85R* and *pk1/+;G85R* (with TTX alone, see methods) are qualitatively similar to *G85R* and WT. Stimuli 1 ms in duration were delivered at 1 Hz, increasing in intensity from 1× to 2× threshold voltage. GCaMP (top, green) fluorescence remains at baseline during stimulation in all genotypes. Gray scale bar between the GCaMP and efEJP traces indicates time scale, time of stimulus (1/second), and stimulus intensity for the GCaMP and top efEJP trace. Expanded efEJP traces are responses at 0, 1, 3, and 5 s. (B) Presynaptic GCaMP spikes and efEJP extension are absent in *sple1/+*;*G85R*, indicating that one copy of the *sple1* mutant allele suppresses *Sh* blockade-induced terminal hyperexcitability of *G85R*. Retention of 4-AP-induced *G85R* hyperexcitability characteristics (GCaMP spikes and extended efEJP) in *pk1/+*;*G85R* demonstrates that the interaction of *sple1* with *G85R* is *prickle* allele-dependent. Arrowheads indicate efEJP "shoulder" characteristic in *G85R* and *pk1/+*;*G85R*.

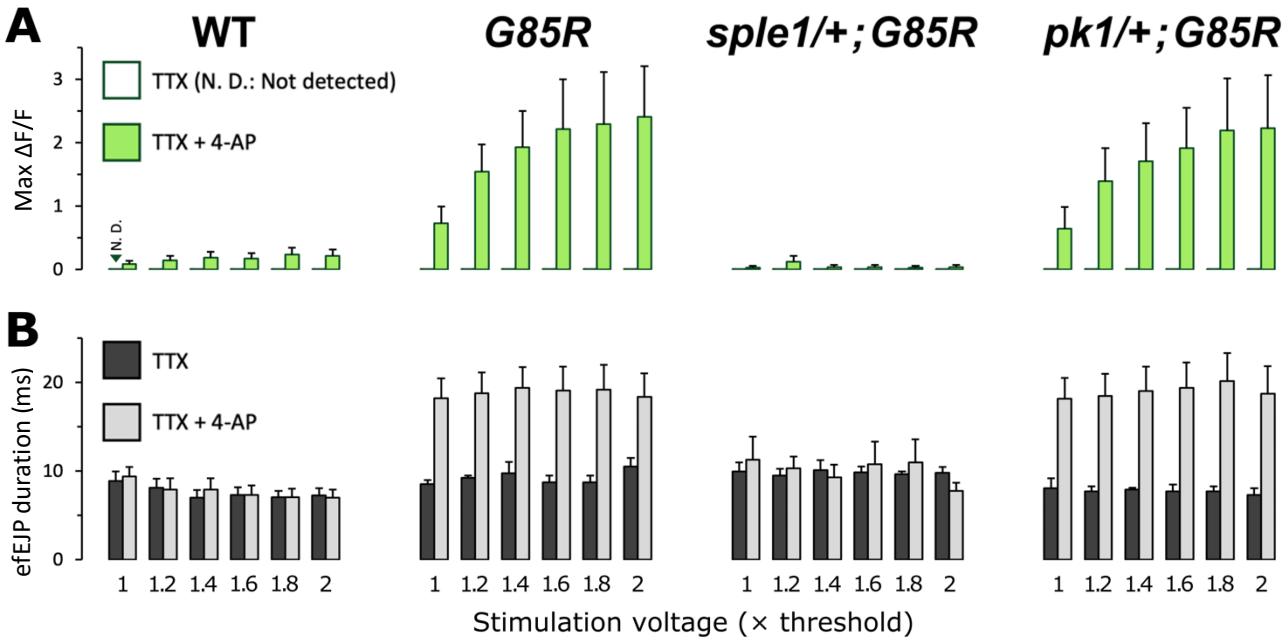

Figure 5. Quantification of presynaptic GCaMP signal amplitude and efEJP duration in *G85R* and *pk*/+;*G85R* double-mutants. (A) Mean GCaMP signal amplitudes (peak ΔF/F) in response to 1 Hz stimuli, of intensity from 1× to 2× threshold voltage. Error bars indicate SEM. In the presence of TTX alone, GCaMP signals were always undetectable (no deviation from baseline). Thin dark green line indicates baseline. 4-AP induced large single stimulus-evoked GCaMP spikes (light green bars) in *G85R* and *pk1*/+;*G85R* larvae. WT and *sple1*/+;*G85R* larvae typically lacked these spikes. See GCaMP traces in Figure 6. (B) Mean durations (ms) of the efEJP co-occurring with the GCaMP signals quantified above. efEJP traces were measured at 20% amplitude (see methods). WT and *sple1*/+;*G85R* larvae displayed efEJP of similar duration in the absence (dark gray bars) or presence (light gray bars) of 4-AP. *G85R* and *pk1*/+;*G85R* efEJP under 4-AP were typically about twice the duration of efEJP without 4-AP. The efEJPs of extended duration were those displaying the shoulder-like characteristic indicated in Figure 6.

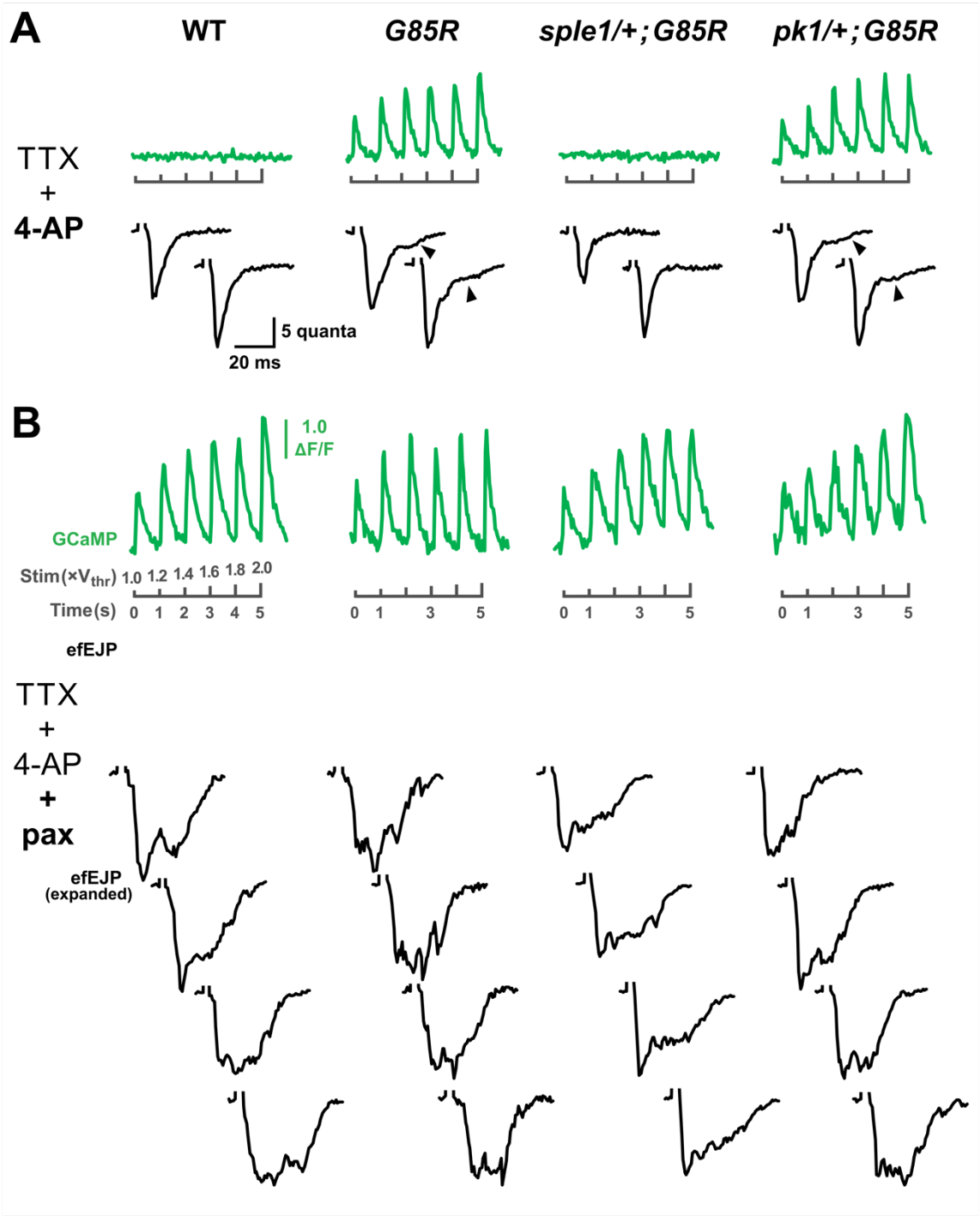
A
WT
G85R
sple1/+;G85R
pk1/+;G85R
TTX
+
4-AP
5 quanta
20 ms
B
1.0
ΔF/F
GCaMP
Stim(×Vthr) 1.0 1.2 1.4 1.6 1.8 2.0
Time(s) 0 1 2 3 4 5
0 1 3 5
0 1 3 5
0 1 3 5
efEJP
TTX
+
4-AP
+
pax
efEJP
(expanded)

Figure 6. Blockade of *slowpoke* BK channels in addition to *Shaker* channels produces extreme motor terminal hyperexcitability. (A) GCaMP and efEJP traces from the TTX + 4-AP condition for WT, *G85R, sple1*/+;*G85R*, and *pk1*/+;*G85R* are shown for comparison to panel B. Expanded efEJP traces are responses at 1, 3 s. (See Figure 6 for additional and more thorough representation.) (B) Blockade of *Sh* and *slo* K^+ channels, by 4-AP and paxilline respectively, produces extreme terminal hyperexcitability that shares characteristics with the hyperexcitability observed in *G85R* and *pk1*/+;*G85R* under the influence of 4-AP alone. Paxilline-induced terminal hyperexcitability is qualitatively similar across all genotypes examined.

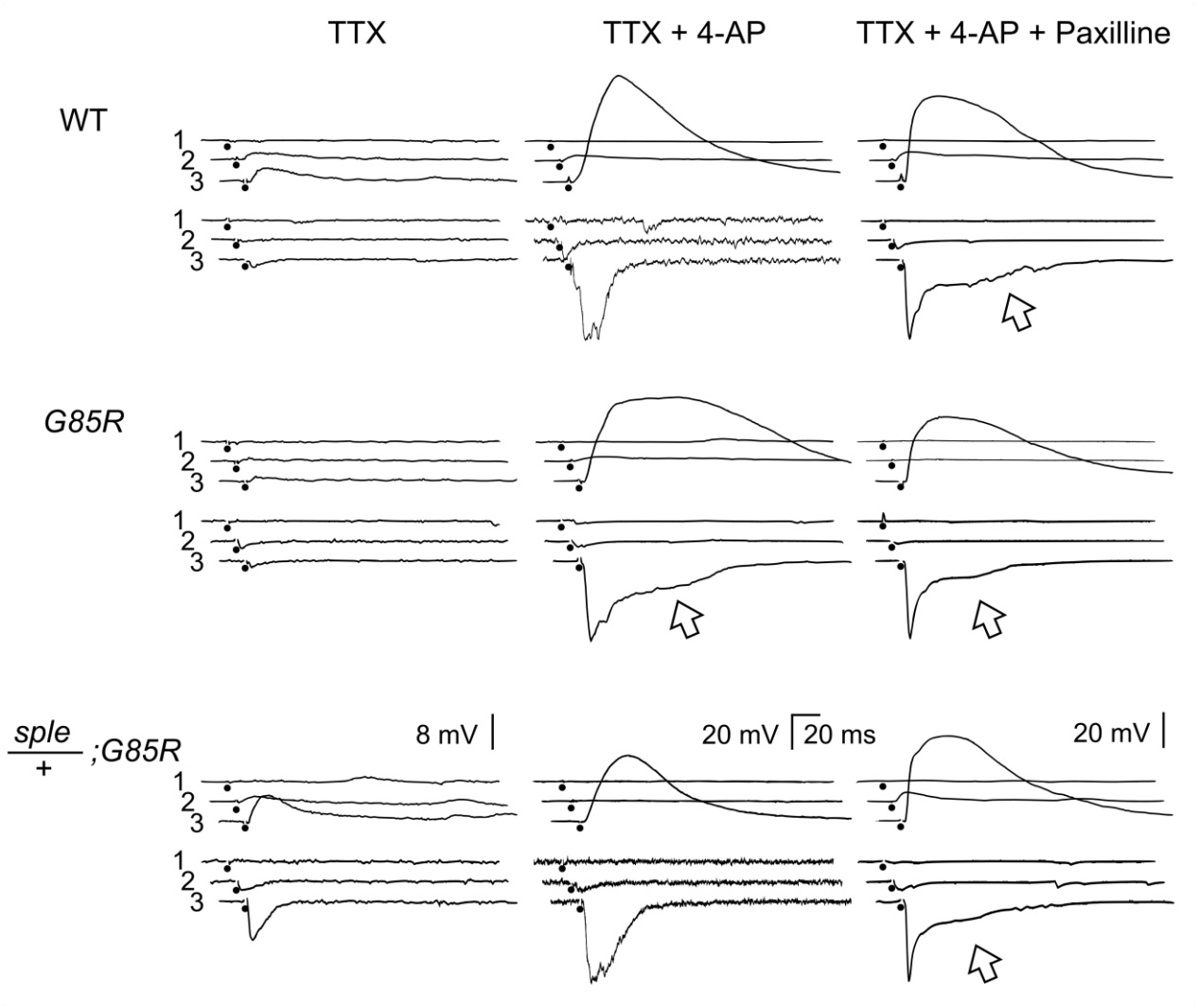

Figure 7. Extended NMJ transmission in *G85R* broadens whole-cell EJPs in the postsynaptic muscle, and heterozygous *sple1* ameliorates this phenotype. Double-recording of whole-cell EJPs and extracellular macropatch EJPs induced by electrotonic depolarization (●) of nerve terminals in the presence of TTX. Application of 4-AP increased the size of EJPs in all genotype. Note that sod^{G85R} exhibited broadened whole-cell EJPs associated with a shoulder of macropatch EJPs (arrow), while WT and $pk^{sple}/+;sod^{G85R}$ lacked them. Application of paxilline induced broadened whole-cell EJPs plus a shoulder of macropatch EJPs (arrow) in all genotypes. 1, 2, 3 indicates sub-threshold, near threshold, and supra-threshold (x3 ~ x5) stimulation. Macropatch EJP traces are normalized.